

Journal of Materials Chemistry A

Accepted Manuscript



This is an *Accepted Manuscript*, which has been through the Royal Society of Chemistry peer review process and has been accepted for publication.

Accepted Manuscripts are published online shortly after acceptance, before technical editing, formatting and proof reading. Using this free service, authors can make their results available to the community, in citable form, before we publish the edited article. We will replace this *Accepted Manuscript* with the edited and formatted *Advance Article* as soon as it is available.

You can find more information about *Accepted Manuscripts* in the [Information for Authors](#).

Please note that technical editing may introduce minor changes to the text and/or graphics, which may alter content. The journal's standard [Terms & Conditions](#) and the [Ethical guidelines](#) still apply. In no event shall the Royal Society of Chemistry be held responsible for any errors or omissions in this *Accepted Manuscript* or any consequences arising from the use of any information it contains.

COMMUNICATION

Metallic Ni Nanocatalyst *in situ* Formed from a Metal-Organic-Framework by Mechanochemical Reaction for Hydrogen Storage in Magnesium

Cite this: DOI: 10.1039/x0xx00000x

Received 00th January 2012,
Accepted 00th January 2012Yi Jia,^{a,b,c} Chenghua Sun,^e Ye Peng,^{c,e} Wenqi Fang,^c Xuecheng Yan,^c Dongjiang Yang,^c Jin Zou,^b Samuel S. Mao,^f and Xiangdong Yao^{*a,c}

DOI: 10.1039/x0xx00000x

www.rsc.org/

Facile and scalable fabrication of ultrafine (<5 nm) nanoparticles (NPs) as effective catalysts is a key for enhancing kinetics in application of most hydrogen storage materials (HSMs). The direct fabrication of ultrafine NPs in HSMs is obviously a challenge because of inevitable NPs agglomeration during thermo-reduction. Here, we demonstrate a mechanochemical-force-driven procedure for one-step preparing Ni NPs (2-3 nm) in MgH₂ matrix, which capitalizes on the *in-situ* bottom-up reduction of Ni-MOF-74 in the presence of MgH₂ as reducing and sacrificing agent under room temperature. Both theoretical calculation and experimental investigations elucidate that ultrafine Ni NPs are much more effective on catalytic hydrogenation/dehydrogenation in Mg due to the size effect. Prospectively, our finding may facilitate the fabrication of other catalyzed HSMs by using different MOFs as catalyst precursors.

Hydrogen is an ideal clean carrier for storage and conversion of energy to meet zero greenhouse gas emission and release the dependence on fossil fuel. A big challenge for widespread use of hydrogen is to develop safe, efficient and high-density hydrogen storage technologies. Magnesium hydride (MgH₂) has been attracted numerous interest for hydrogen storage in the last several decades due to its high hydrogen capacity (7.7 wt%), excellent reversibility, abundance, low cost and non-toxicity.¹ However, its use as a practical hydrogen storage material has been impeded by high dehydrogenation thermal stability ($\Delta H=75$ kJ/mol H₂) and slow sorption kinetics, leading to that MgH₂ must be heated to 300-400 °C to achieve an adequate rate of dehydrating and hydrating.²⁻⁶ A number of strategies have been developed to overcome these disadvantages that are essentially imposed by the strong Mg-H chemical bonds, such as nanostructuring,⁷⁻¹² catalyzing¹³⁻¹⁶ and alloying.¹⁷⁻²¹ A wide range of metals¹⁵ and their alternatives¹⁶ have been demonstrated to be effective for enhancing the de/hydrogenation properties when ball-milled with Mg to form nanocomposites. Moreover, a general consensus is that size effect of catalysts doping plays critical roles in fabricating catalyzed Mg-

based nanocomposites, including several advantages such as reducing the fabrication cost (catalysts adding amount and milling time) and enhancing de/hydrogenation due to increased Mg-catalysts interfaces.⁵ One of the most notable reported studies was Ni^{nano} (diameter of several tens of nanometers) doped MgH₂ composite prepared by mechanical milling, exhibiting substantially improved kinetics of dehydrogenation compared to undoped MgH₂, which shows the importance of size effect of doped catalyst.¹⁵ To further investigate the size effect of catalyst doping, various carbon supported metallic Ni nanocatalysts with smaller particles size in the range of 8-100 nm have been successfully synthesized and utilized to dope in MgH₂ matrix via ball milling for enhanced hydrogen sorption performance.²²⁻²⁵ However, most carbon supported metallic Ni nanocatalysts synthesized by wet chemistry usually require relative high calcination temperature (500-600 °C) to complete the reduction process, which will be inevitable to lead to agglomeration of partial catalyst particles. It is remarkable that such particles agglomeration may reduce the surface catalytic activity comparing with smaller metallic catalysts due to the size effect.²⁶

Recently, based on a newly emerging *in-situ* bottom-up synthetic method, the metal-organic frameworks (MOFs) self-assembled by the coordination of metal cations/clusters with organic linkers have been considered as ideal precursors to fabricate uniform ultrafine metallic nanoparticles under proper thermolysis conditions.²⁷ These as-generated ultrafine metallic nanoparticles could sever as efficient catalysts in de/hydrogenation process when they were dispersed in MgH₂ matrix homogenously. Alternatively, the mechanochemical synthesis strategy is a low cost and scalable solution for the synthesis of a wide range of ultrafine nanoparticles (<4 nm) as catalysts since the nature of mechanochemical synthesis involves a simultaneous combination of chemical reaction and materials dispersion.⁸ However, the main hurdle encountering in current mechanochemical synthesis is that extra inert buffering material (usually a reaction byproduct phase) needs to be added to the reagents for enhancing product phase separation to get desired ultrafine nanoparticles.²⁸ It is noted that the removal of inert buffering materials may not only increase the fabrication cost but also lead to nanoparticles agglomeration. Therefore, exploring and developing novel synthesis methods for preparation and stabilization

of ultrafine metallic nanocatalysts in MgH_2 matrix in a single step is highly desirable for achieving improved hydrogen storage properties for practical applications.

Herein, in this work, we present a one-step mechanochemical synthesis method to prepare ultrafine metallic Ni nanoparticles where were directly dispersed in the active buffering materials, namely the targeted MgH_2 matrix (denoted as (Ni-NPs)@ MgH_2). The resultant (Ni-NPs)@ MgH_2 capitalized on the *in-situ* bottom-up reduction of Ni-MOF-74 precursor in the presence of MgH_2 as reducing and sacrificing agent via mechanochemical ball milling under room temperature. As a proof of principles, ultrafine Ni nanoparticles measuring 2-3 nm were successfully prepared and embedded in crushed MgH_2 matrix. More importantly, the (Ni-NPs)@ MgH_2 composite with only 5 wt% Ni-MOF-74 adding amount showed ultrafast kinetics and very high capacity at low temperatures. The promoted de/hydrogenation performance is attributed to the uniform dispersion of *in-situ* generated ultrafine Ni nanocatalyst, which was proved by the theoretical calculation and comparison experiments. Potentially, such a technique may be extended to prepare uniform and ultrafine nanocatalysts in other hydrogen storage metal/complex hydrides for scalable synthesis.

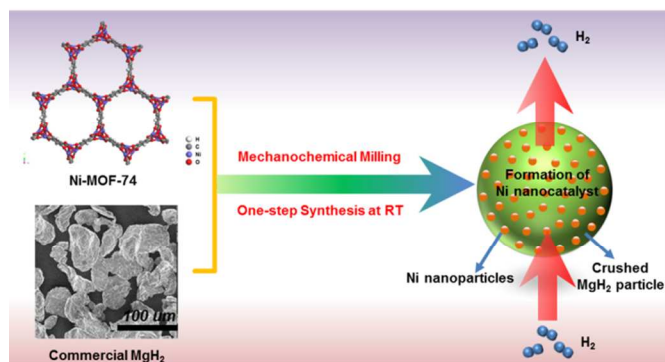


Fig. 1 Schematic of mechanochemical synthesis of (Ni-NPs)@ MgH_2 composite: formation of ultrafine Ni nanoparticles embedded in crushed MgH_2 particles by ball milling of Ni-MOF-74 and commercial MgH_2 .

Fig. 1 presents a schematic diagram of (Ni-NPs)@ MgH_2 composite preparation: formation of ultrafine Ni nanoparticles embedded in crushed MgH_2 particles. The molecular structure of Ni-MOF-74 ($\text{C}_8\text{H}_2\text{O}_6\text{Ni}_2$) as a Ni precursor (Fig. 1) presents the unique advantage of coordinate Ni sites with porous framework structure, which is expected to benefit *in-situ* reduction of Ni NPs in the period of mechanochemical ball milling process due to the large surface area.²⁹ Firstly, the BET surface area, micropore volume and micropore size of Ni-MOF-74 are measured by N_2 adsorption isotherms, which are $614 \text{ m}^2 \text{ g}^{-1}$, $0.34 \text{ cm}^3 \text{ g}^{-1}$ and 0.93 nm , respectively (Fig. S1). These data are very close to the values reported by other groups, suggesting that Ni-MOF-74 was correctly synthesized.²⁹ Afterwards, the as-prepared Ni-MOF-74 as the Ni precursor was mixed with commercial MgH_2 powders, and then ball milled under 1 bar Ar for 2 h in a high-energy ball mill (SPEX 8000) within a sealed vial by the ball-to-powder weight ratio of 40:1. To study the evolution of sample phases after ball milling, a batch of as-milled samples (5, 20 and 50 wt% adding level of Ni-MOF-74) has been characterized by powder X-ray diffraction (XRD). Based on the XRD patterns in Fig. 2A, it is noteworthy that the characteristic peaks of Ni-MOF-74 (pattern a in Fig. 2A) were diminished after ball milling process. Besides the typical tetragonal $\beta\text{-MgH}_2$ (JCPDS 12-0697) and meta-stable orthorhombic phase $\gamma\text{-MgH}_2$ (JCPDS 35-1184) phases, a small and broad peak of Ni (111) can be clearly

identified in the as-milled MgH_2 +5 wt% (Ni-MOF-74) sample (pattern b in Fig. 2A). The mean grain size is 3.6 nm estimated by Sherrer equation. This clearly indicates that ultrafine Ni nanoparticles were generated due to the *in-situ* reduction of Ni-MOF-74 in the period of ball milling process. Furthermore, 20 wt% adding amount of Ni-MOF-74 (pattern c in Fig. 2A) leads to more intense Ni peak than that of 5 wt% counterpart, albeit at the expense of MgO phase observed. More importantly, with further increasing the Ni-MOF-74 adding amount to 50 wt%, MgH_2 is completely oxidized to MgO (pattern d in Fig. 2A), suggesting the control of adding amount of Ni-MOF-74 is critical to the (Ni-NPs)@ MgH_2 composite preparation. To further confirm the *in-situ* reduction between MgH_2 and Ni-MOF-74 in the period of ball milling process, X-ray photoelectron spectrometer (XPS) technique was employed to investigate into the surface chemical composition of as-milled MgH_2 +5 wt% (Ni-MOF-74) composite, to obtain clear valence evolution of Ni in various states. As shown in Ni-MOF-74 sample (pattern a in Fig. 2B), the binding energy of Ni $2p_{3/2}$ peak of 855.1 eV coincides with the valence state of Ni (2+) in Ni-MOF-74. Whereas the major Ni $2p_{3/2}$ peak shifted down to lower binding energy of 852.1 eV in as-milled MgH_2 +5 wt% (Ni-MOF-74) sample, partial Ni $2p_{3/2}$ peak at 855.1 eV preserved (as shown in pattern b in Fig. 2B). It is suggested that Ni (0) metal was formed after the reaction of MgH_2 and Ni-MOF-74, which is coincided with XRD results. In order to investigate the microstructure of Ni NPs in as-milled (Ni-NPs)@ MgH_2 composite, high resolution transmission electron microscope (HRTEM) and energy dispersive X-ray spectroscopy (EDXs) techniques are employed. HRTEM image of MgH_2 +5 wt% (Ni-MOF-74) sample (Fig. 2C inset) clearly shows that the ultrafine Ni (111) NPs with particles size of 2-3 nm were embedded in MgH_2 matrix. Furthermore, the dispersion of Ni NPs in MgH_2 matrix is identified by EDXs in Fig. 2D, which shows Ni element existing in the different randomly selected spots among the matrix (Fig. 2C). This suggests that the *in-situ* reduced ultrafine Ni NPs (2-3 nm) are uniformly distributed in the MgH_2 based composite after mechanochemical synthesis.

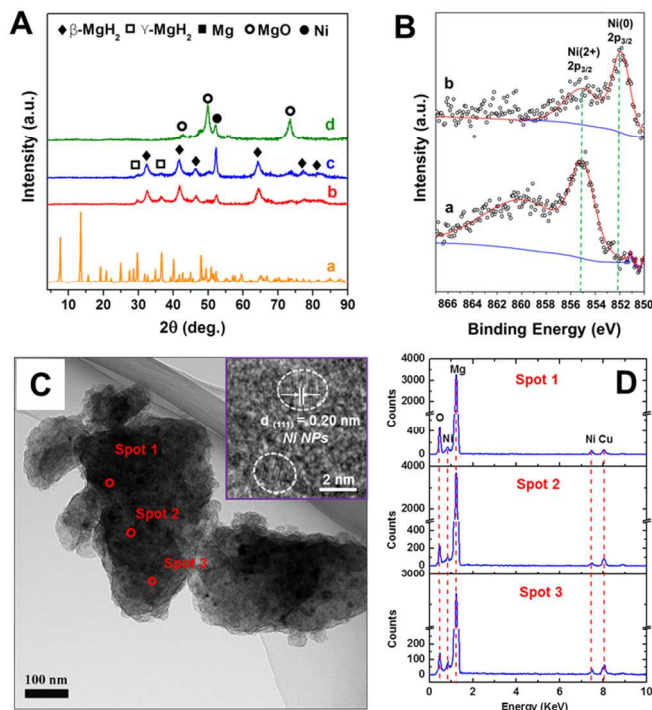


Fig.2 Characterization of as-milled (Ni-NPs)@MgH₂ composites: (A) XRD patterns of Ni-MOF-74 and as-milled samples (a) Ni-MOF-74, (b) MgH₂+5%(Ni-MOF-74), (c) MgH₂+20%(Ni-MOF-74), (d) MgH₂+50%(Ni-MOF-74); (B) XPS spectra of Ni 2p_{3/2} of (a) Ni-MOF-74, (b) as-milled MgH₂+5%(Ni-MOF-74); (C) TEM image of as-milled MgH₂+5%(Ni-MOF-74) with inset high resolution TEM (HRTEM) of Ni NPs and (D) EDXs analysis of selected spots in C.

Fig. 3a and b illustrate the hydrogenation/dehydrogenation kinetics of the as-prepared (Ni-NPs)@MgH₂ (MgH₂+5 wt% (Ni-MOF-74)) sample at different temperatures under a hydrogen pressure of 2 MPa for hydrogen absorption and 1 KPa for dehydrogenation. As shown in Fig. 3a, the composites can absorb 6.2 wt% hydrogen within only 30 s at a temperature as low as 150 °C. Furthermore, the composite can even absorb 4.4 wt% hydrogen at 100 °C within only 10 min. More interestingly, even under room temperature (RT), MgH₂+5 wt% (Ni-MOF-74) composite can still take up 2.7 wt% hydrogen within 10 h (Fig 3a inset). The ultrafast kinetics for hydrogen absorption at low temperatures is very significant for practical applications. To our best knowledge, our result of hydrogen storage under RT is very close the current best record (store 3 wt% hydrogen within 4 h under a hydrogen pressure of 2 MPa) reported by Lu et al. using TiH₂ as catalyst.³⁰ It is remarkable that the additive amount in this work is much less (5 wt% Ni-MOF-74 vs 16 wt% TiH₂) for cutting fabrication cost and remaining high theoretical hydrogen storage capacity of the system. With respect to hydrogen desorption, the MgH₂+5 wt% (Ni-MOF-74) composite shows reasonably good kinetics even at relatively lower temperatures (300, 280 and 260 °C) as shown in Fig. 3b. The composite can fully desorb 6.2 wt% hydrogen within just 20 min at 300 °C, and can desorb 4.5 wt% hydrogen at 280 °C and desorb 3 wt% hydrogen at 260 °C within 20 min, respectively.

Based on the XRD result, MgO will be formed as the by-product during the *in-situ* reduction of Ni NPs in MgH₂ matrix. Therefore, increasing the adding amount of Ni-MOF-74 precursor may reduce the hydrogen storage capacity of the composites as more Mg, the hydrogen sorbent, will be oxidized. As shown in Fig. 3c, it is observed that the significant decrease of the practical hydrogen absorption capacity from 4.4 wt% (5 wt% adding level of Ni-MOF-74) to 2.5 wt% (20 wt% adding level of Ni-MOF-74) at 100 °C (10 minutes). Furthermore, the rehydrogenated (Ni-NPs)@MgH₂ samples (5 wt% and 20 wt% adding level of Ni-MOF-74, hydrogenation under 2 MPa, 1 h, 100 °C) are characterized by XRD (Fig. S2), it shows that the major content is from β-MgH₂ (JCPDS 12-0697) in rehydrogenated states, together with a small amount of residual Mg phase, indicating most of Mg phase has transformed into β-MgH₂ phase at such a temperature as low as 100 °C. Meanwhile, in Fig 3c, it is not surprising that there is almost no hydrogen absorption from (Ni-NPs)@MgH₂ with 50 wt% adding amount of Ni-MOF-74 even at 200 °C due to the massive formation of MgO, which is also consistent with XRD results. Additionally, the existence of increased amount of MgO also inhibits the kinetics in hydrogen absorption, which is evidenced by better absorption kinetics of (Ni-NPs)@MgH₂ with lower adding level of Ni-MOF-74 as seen in Fig 3c. In terms of hydrogen desorption, it is also interesting that although the desorption practical hydrogen capacity of (Ni-NPs)@MgH₂ was reduced from 6.2 wt% (5 wt% adding level of Ni-MOF-74) to 4.8 wt% (20 wt% adding level of Ni-MOF-74) within 1h at 300 °C, there is no obvious effect on desorption kinetics as shown in Fig. 3d. All these results demonstrate that (1) the *in-situ* reduced ultrafine Ni catalyst is very active and effective, enabling a small adding level of Ni-MOF-74 precursor (5 wt%) and superior

catalytic effect on MgH₂ de/hydrogenation; (2) increasing adding amount of Ni-MOF-74 precursor (20 and 50 wt%) will hinder the catalytic effect in both absorption and desorption due to the formation of MgO.

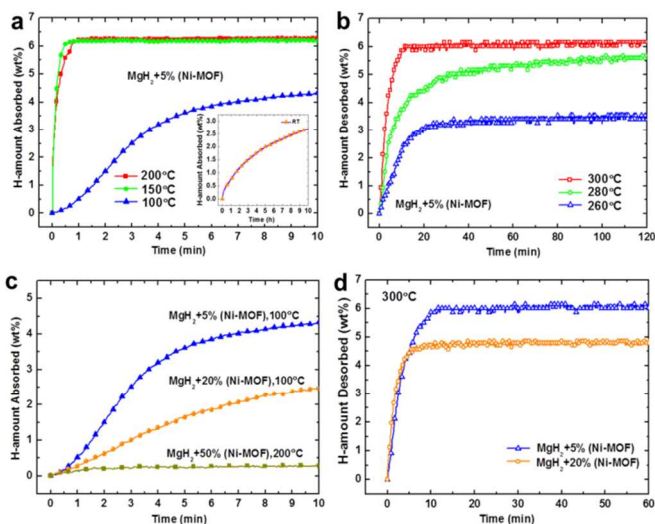


Fig.3 Hydrogen absorption/desorption performance of (Ni-NPs)@MgH₂ composites: effect of different temperatures on (a) hydrogen absorption and (b) desorption kinetics of MgH₂+5 wt% (Ni-MOF-74) sample; effect of different adding amount of Ni-MOF-74 precursor on (c) hydrogen absorption and (d) desorption kinetics of (Ni-NPs)@MgH₂ composites.

To improve hydrogen ab/desorption from MgH₂, transition metals (TMs)-doping have been considered by several groups.^{31,32} Previously, theoretical calculations indicated that Pd-doping can significantly reduce the barrier for H₂ dissociation and diffusion of atomic H, which are the key factors to determine the hydrogenation/dehydrogenation kinetics of MgH₂.³¹ With single Pd-incorporation into Mg(0001) surface, the dissociation barrier is reduced from 1.05 eV to 0.31 eV.³¹ Pozzo et al. carried out a more comprehensive investigation of TMs doping, including Ti, Zr, V, Fe, Ru, Co, Rh, Ni, Pd, Cu and Ag, and identified the most promising dopants would be Ni, Fe and Rh based on calculated barriers.³² Most of these calculations were based on a model with single dopant replacing magnesium at the lattice site, in which case the diffusion of single hydrogen atom over dopants cannot be fully investigated. As strong TM-H may be presented, as a result, hydrogen may hardly shift from dopants to the magnesium matrix. This would be a big problem since the active sites of dopants will be covered by dissociated H atoms quickly and thus be poisoned for following reactions due to size dependant H diffusion rate on dopants. Therefore, ideal dopants should offer moderate bonding with hydrogen and small size. In addition, single-atom incorporation model may lead to local strain energy and activate the neighbouring magnesium, leading to artificial improvement.

To rule out such effect, we particularly introduce a cluster Ni₄ on Mg(0001), as shown in Fig. 4a, followed by full relaxation to release the strain energy. The reason why such small cluster is employed has been justified in the supporting information. H₂ is then adsorbed on the cluster with dissociated form. We focused on the diffusion of atomic hydrogen. Fig. 4b presents the energy profile, from which an energy barrier of 0.41 eV has been identified. In addition, shifting one hydrogen from Ni-cluster to Mg(0001) only leads to an energy increment of 0.07 eV, indicating dissociated hydrogen can quickly

shift from those active sites to pure Mg(0001), and the later shows excellent performance for surface diffusion ($E_a < 0.20$ eV).^{31,32} For dehydrogenation process, hydrogen atoms, after being released from magnesium matrix, can diffuse to those active sites of dopants cluster and recombine with a small barrier (0.30 eV). Here, our results do not generate different conclusions from the model of single-dopant incorporation. This may be attributed to enhanced H₂ dissociation process due to more atomic H dissociated on cluster Ni₄ model comparing with single Ni-atom incorporation model, albeit at the expense of slower H atom diffusion. Following this speculation, atomic H diffusion on Ni cluster may become the rate limiting step (RLS) for de/hydrogenation kinetics if the cluster size are not small enough, which is the basis for fast hydrogenation and dehydrogenation of MgH₂ at moderate temperatures.

In terms of the dehydrogenation, besides the size effect,³³⁻³⁶ another possible improvement may be achieved due to the electron transfer from Mg matrix to Ni-cluster. Recently, we confirmed that a small part of hydrogen can be released below 80 °C from MgH₂ clusters when they are confined in mesoporous carbon, and partially transferring electrons from Mg-matrix is the key reason for such improvement.³⁷ In the case of Ni-adsorption, electrons can also transfer from Mg matrix to Ni-cluster through the strong Ni-Mg interaction; as a result, electrons donated from Mg to H will slightly decrease over those sites close to the Ni-cluster. Such competition between Ni and H, both as electron acceptor, may bring the similar improvement for the dehydrogenation of MgH₂, as we obtained from MgH₂ confined in the carbon-framework.

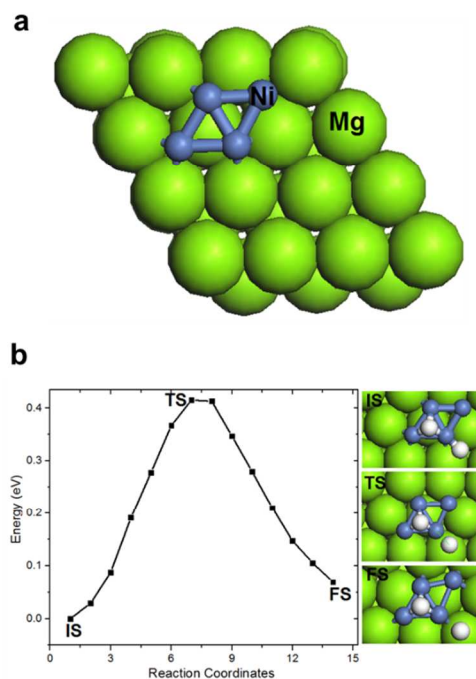


Fig.4 (a) Mg(0001) modelled by the (3×3) supercell, with Ni₄ cluster adsorbed; (b) Energy profile for atomic hydrogen (white spheres) diffusing from Ni₄ to Mg(0001) with the structures of initial state (IS), transition state (TS) and final state (FS). Energy difference between TS and IS indicates the barrier for such diffusion.

To experimentally study the size effect of ultrafine Ni NPs on catalytic mechanism of hydrogenation/dehydrogenation in Mg, we prepared the activated carbon supported Ni nanocatalyst synthesized by wet chemistry method for comparison.²² The Ni content in Ni-MOF-74 was determined by TGA analysis as shown in Fig. S3. It is observed that the TGA curve exhibited a gradual weight-loss step of

22.5 wt% up to 300 °C, corresponding to the removal of solvent molecules (water and DMF) from its microporous structure.²⁹ The second steep weight loss of 37.5 wt%, between 300 and 350 °C, can be ascribed to the decomposition of Ni-MOF-74 due to the organic ligand decomposition. Assuming all the residual (NiO) is from Ni-MOF-74, it can be calculated that Ni content in as-synthesized Ni-MOF-74 is 39.1 wt% which is very close to the theoretical value of 37.7 wt% from stoichiometric formula of Ni-MOF-74 (C₈H₂O₆Ni₂). Therefore, based on the TGA result, 40 wt% Ni loading amount was selected to prepare activated carbon supported Ni nanocatalyst (denoted as Ni/AC) in accordance with Ni content in Ni-MOF-74 (39.1 wt%) for comparison, and both adding amount are in the presence of 5 wt% into MgH₂. TEM bright-field image showed that the particle size of Ni in Ni/AC catalyst was around 10 nm (Fig. S4), which is similar to previous reports.^{22,24} In the comparative study of hydrogen storage, as shown in Fig. 5a, (Ni-NPs)@MgH₂ can absorb 3 wt% hydrogen whereas MgH₂+Ni/AC only absorb 1 wt% hydrogen within 210 s at 100 °C, which is nearly 3-fold faster absorption rate. In terms of desorption, Fig. 5b shows that (Ni-NPs)@MgH₂ also exhibits better catalytic effect as compared to MgH₂+Ni/AC, which is about twice faster (10 min Vs 20 min) to completely desorb 6.2 wt% hydrogen at 300 °C. Therefore, we postulate that nanostructuring of Ni catalyst in (Ni-NPs)@MgH₂ nanocomposite enhances the kinetics for absorption and release of hydrogen. To assess this, we have determined the activation energies (E_a) from analysis of the absorption and release of hydrogen at three different temperatures (Fig. S5). We measure E_a values of 32.5 and 80.5 kJ mol⁻¹ for absorption and desorption in (Ni-NPs)@MgH₂, respectively, which lower than those of MgH₂+Ni/AC (43.8 and 110.8 kJ mol⁻¹ for absorption and desorption, respectively). To further elucidate the size effect of Ni catalyst, we plotted and compared absorption/desorption E_a with more different Ni catalyst dimensions for (Ni-NPs)@MgH₂ (*in situ* reduced Ni from Ni-MOF-74, Ni NPs 2-3 nm, in this work), MgH₂+Ni/AC (activated carbon supported Ni, Ni NPs ~10 nm, in this work), MgH₂+Ni/rGO (reduced graphene oxide supported Ni, Ni NPs ~10 nm, data from ref²⁵) and MgH₂+NiCNFs (nickel coated carbon nanofibers, Ni NPs ~100 nm, data from ref²³) nanocomposites as shown in Fig. 5c. The overall trend clearly shows that both absorption and desorption activation energies (E_a) significantly decrease with reducing the Ni catalyst size from 100 nm to 2-3 nm, implying the size effect of catalyst can significantly promote hydrogen absorption/desorption kinetics. All these results demonstrate that hydrogen storage properties of (Ni-NPs)@MgH₂ composite is superior, which may ascribe to ultrafine Ni NPs (2-3 nm) uniformly embedded in (Ni-NPs)@MgH₂ composite.

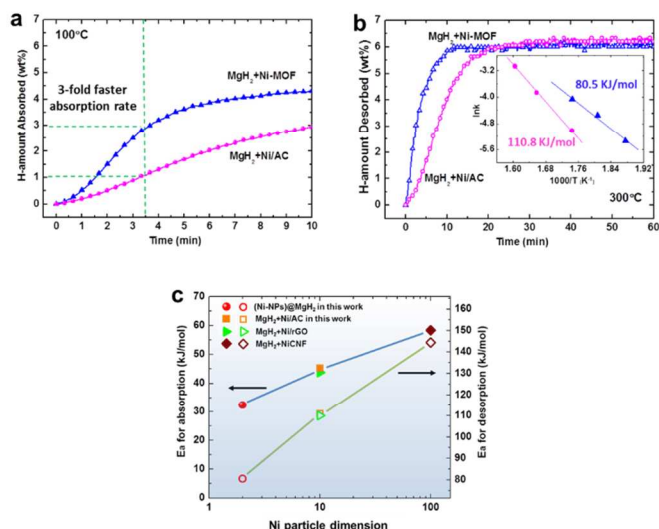


Fig.5 Size effect of Ni-NPs on (a) hydrogen absorption, (b) desorption performance in (Ni-NPs)@MgH₂ and MgH₂+Ni/AC with inset arrhenius plot for the dehydrogenation kinetics and (c) comparison in absorption/desorption activation energies (E_a) and Ni catalyst dimensions for (Ni-NPs)@MgH₂ (*in situ* reduced Ni from Ni-MOF-74, Ni NPs 2-3 nm, in this work), MgH₂+Ni/AC (activated carbon supported Ni, Ni NPs ~10 nm, in this work), MgH₂+Ni/rGO (reduced graphene oxide supported Ni, Ni NPs ~10 nm, data from ref²⁵) and MgH₂+NiCNFs (nickel coated carbon nanofibers, Ni NPs ~100 nm, data from ref²³) nanocomposites.

Conclusions

In summary, we have developed a one-step mechanochemical synthesis method to prepare ultrafine metallic Ni nanoparticles (2-3 nm) in MgH₂ matrix (denoted as (Ni-NPs)@MgH₂). Our approach capitalises on the *in-situ* bottom-up reduction of Ni-MOF-74 precursor in the presence of MgH₂ as reducing and sacrificing agent via mechanochemical ball milling under room temperature. The hydrogen storage properties of the (Ni-NPs)@MgH₂ nanocomposite obtained by this technique was superior to those of other Ni doped counterparts, which is evidenced by significantly decreased absorption/desorption activation energies (E_a) with reducing Ni particle dimension from 100 nm to 2-3 nm. Prospectively, this approach of scalable synthesizing uniform and ultrafine nanocatalysts may be applied to preparation of other catalyzed hydrogen storage metal/complex hydrides nanocomposites by using different MOFs as catalyst precursors.

Acknowledgements

The financial support from Australia Research Council (ARC) is appreciated. Dr. Yi Jia also thanks the Griffith University Postdoctoral and Research Fellowship and Griffith University New Research Grant.

Notes and references

^a ARC Centre of Excellence for Functional Nanomaterials, School of Engineering and Australian Institute of Bioengineering and Nanotechnology, University of Queensland, St Lucia, QLD 4072, Australia.

^b School of Mechanical and Mining Engineering, University of Queensland, St Lucia, QLD 4072, Australia.

^c Queensland Micro- and Nanotechnology Centre (QMNC), Griffith University, Nathan, QLD 4111, Australia. Email: x.yao@griffith.edu.au

^d School of Chemistry, Faculty of Science, Monash University, VIC 3800, Australia.

^e State Key Laboratory of Inorganic Synthesis and Preparative Chemistry, Jilin University, Changchun, 130012, P R China.

^f Environmental Energy Technologies Division, Lawrence Berkeley National Laboratory, Department of Mechanical Engineering, University of California at Berkeley, Berkeley, CA94720, United States.

† Electronic Supplementary Information (ESI) available: See DOI: 10.1039/c000000x/

- W. Grochala, P. P. Edwards, *Chemical Reviews*, 2004, **104**, 1283.
- F. Y. Cheng, Z. L. Tao, J. Liang, J. Chen, *Chem. Commun.*, 2012, **48**, 7334.
- A. J. Churchard, E. Banach, A. Borgschulte, R. Caputo, J. C. Chen, D. C. Clary, K. J. Fijalkowski, H. Geerlings, R. V. Genova, W. Grochala, T. Jaron, J. C. Juanes-Marcos, B. Kasemo, G. J. Kroes, I. Ljubic, N. Nadjok, J. K. Norskov, R. A. Olsen, F. Pendolino, A. Remhof, L. Romaszki, A. Tekin, T. Vegge, M. Zach, A. Zuttel, *Phys. Chem. Chem. Phys.*, 2011, **13**, 16955.
- R. Bardhan, A. M. Ruminski, A. Brand, J. J. Urban, *Energy Environ. Sci.*, 2011, **4**, 4882.
- P. E. de Jongh, P. Adelhelm, *ChemSusChem*, 2010, **3**, 1332.
- K. F. Aguey-Zinsou, J. R. Ares-Fernandez, *Energy Environ. Sci.*, 2010, **3**, 526.
- N. S. Norberg, T. S. Arthur, S. J. Fredrick, A. L. Prieto, *J. Am. Chem. Soc.*, 2011, **133**, 10679.
- M. Paskevicius, D. A. Sheppard, C. E. Buckley, *J. Am. Chem. Soc.*, 2010, **132**, 5077.
- S. B. Kalidindi, B. R. Jagirdar, *Inorg. Chem.*, 2009, **48**, 10856.
- I. Haas, A. Gedanken, *Chem. Commun.*, 2008, 1795.
- K. F. Aguey-Zinsou, J. R. Ares-Fernandez, *Chem. Mat.*, 2008, **20**, 376.
- W. Y. Li, C. S. Li, H. Ma, J. Chen, *J. Am. Chem. Soc.*, 2007, **129**, 6710.
- A. Zaluska, L. Zaluski, J. O. Strom-Olsen, *J. Alloy. Compd.*, 1999, **288**, 217.
- G. Liang, J. Huot, S. Boily, A. Van Neste, R. Schulz, *J. Alloy. Compd.*, 1999, **292**, 247.
- N. Hanada, T. Ichikawa, H. Fujii, *J. Phys. Chem. B*, 2005, **109**, 7188.
- G. Barkhordarian, T. Klassen, R. Bormann, *J. Phys. Chem. B*, 2006, **110**, 11020.
- D. Moser, D. J. Bull, T. Sato, D. Noreus, D. Kyoji, T. Sakai, N. Kitamura, H. Yusa, T. Taniguchi, W. P. Kalisvaart, P. Notten, *J. Mater. Chem.*, 2009, **19**, 8150.
- C. X. Shang, M. Bououdina, Y. Song, Z. X. Guo, *Int. J. Hydrog. Energy*, 2004, **29**, 73.

- 19 J. J. Vajo, F. Mertens, C. C. Ahn, R. C. Bowman, B. Fultz, *J. Phys. Chem. B*, 2004, **108**, 13977.
- 20 G. S. Walker, M. Abbas, D. M. Grant, C. Udeh, *Chem. Commun.*, 2011, **47**, 8001.
- 21 C. S. Zhou, Z. G. Z. Fang, J. Lu, X. Y. Zhang, *J. Am. Chem. Soc.*, 2013, **135**, 10982.
- 22 M. A. Lio-Rodenas, K. F. Aguey-Zinsou, D. Cazorla-Amoros, A. Linares-Solano, Z. X. Guo, *J. Phys. Chem. C*, 2008, **112**, 5984.
- 23 C. Z. Wu, X. D. Yao, H. Zhang, *Int. J. Hydrog. Energy*, 2009, **35**, 247.
- 24 Y. Jia, L. N. Cheng, N. Pan, J. Zou, G. Q. Lu, X. D. Yao, *Adv. Energy Mater.*, 2011, **1**, 387.
- 25 G. Liu, Y. J. Wang, F. Y. Qiu, L. Li, L. F. Jiao, H. T. Yuan, *J. Mater. Chem.*, 2012, **22**, 22542.
- 26 E. Roduner, *Chem. Soc. Rev.*, 2006, **35**, 583.
- 27 J. K. Sun, Q. Xu, *Energy Environ. Sci.*, 2014, **7**, 2071.
- 28 P. G. McCormick, T. Tsuzuki, J. S. Robinson, J. Ding, *Adv. Mater.*, 2001, **13**, 1008.
- 29 T. G. Glover, G. W. Peterson, B. J. Schindler, D. Britt, O. Yaghi, *Chem. Eng. Sci.*, 2011, **66**, 163.
- 30 J. Lu, Y. J. Choi, Z. Z. Fang, H. Y. Sohn, E. Ronnebro, *J. Am. Chem. Soc.*, 2010, **132**, 6616.
- 31 A. J. Du, S. C. Smith, X. D. Yao, G. Q. Lu, *J. Am. Chem. Soc.*, 2007, **129**, 10201.
- 32 M. Pozzo, D. Alfe, *Int. J. Hydrog. Energy*, 2009, **34**, 1922.
- 33 X. Y. Lai, J. E. Halpert, D. Wang, *Energy Environ. Sci.*, 2012, **5**, 5604.
- 34 N. L. Yang, Q. Yuan, J. Zhai, T. X. Wei, D. Wang, L. Jiang, *ChemSusChem*, 2012, **5**, 572.
- 35 D. Wang, H. H. Tong, H. Y. Xu, Y. Matsumura, *Catal. Today*, 2004, **93**, 689.
- 36 J. H. Tong, H. Y. Xu, D. Wang, Y. Matsumura, *J. Jpn. Pet. Inst.*, 2004, **47**, 64.
- 37 Y. Jia, C. H. Sun, L. N. Cheng, M. A. Wahab, J. Cui, J. Zou, M. Zhu, X. D. Yao, *Phys. Chem. Chem. Phys.*, 2013, **15**, 5814.